International Journal of Multidisciplinary Research and Development
Online ISSN: 2349-4182 Print ISSN: 2349-5979
www.allsubjectjournal.com
Volume 3; Issue 1; January 2016; Page No. 294-303

Thermophoresis effect on mixed convection flow from a rotating cone embedded in a porous medium with thermal radiation

[1] Dr. Sreedhar Babu M, [2] Lavanya M, [3] Venkata Ramanaiah G

[1] Asst. professor, Dept. of Applied Mathematics, Y.V. University, Kadapa, Andhra Pradesh, India.

[2, 3] Research scholar, Dept. of Applied Mathematics, Y.V. University, Kadapa, Andhra Pradesh, India.

Abstract
In this paper we analyzed the study of steady, laminar, incompressible convection flow along a rotating vertical cone with thermal radiation and thermophoresis immersed in a fluid saturated porous medium. The fluid is assumed to be a gray, absorbing-emitting but a scattering medium. The radiative heat flux in the energy equations is described by employing the Rosseland approximation. The governing equations for the conservation of mass, momentum, energy and concentration of the problem are formulated. The resultant equations are transformed into simple ordinary non-linear differential equations and then solved by employing Runge-Kutta method with shooting technique. The numerical results concerning the flow fields, such as, the fluid velocities (tangential, circumferential and normal), temperature and concentration profiles across the boundary layer are discussed graphically for different values of physical parameters, namely thermophoresis coefficient, relative temperature difference parameter, inverse Darcy parameter and thermal radiation. These characteristics are also discussed with the aid of Nusselt number and Sherwood number. It is noted that the results are compared with earlier existing results.

Keywords: Rotating cone, porous medium, thermophoresis, thermal radiation.

1. Introduction

Problems of coupled heat and mass transfer from different geometries embedded in porous media have great importance in numerous engineering and industrial processes such as thermal insulation, underground energy transportation, drying of porous solids, enhanced oil recovery and cooling of nuclear reactors. Few models of these processes are design of chemical processing equipment, cooling towers, food process, harm of crops due to freezing, desalination, refrigeration and air conditioning, consolidated heat exchangers, solar power collectors, etc. References of comprehensive literature surveys concerning the topic of porous media can be had in most recent books by Nield and Bejan [14], Vafai [21], Pop and Ingham [16], and Ingham and Pop [11]. Further, A phenomenon which origins small particles to be vigorous away from a hot surface and towards a cold one is well-known as thermophoresis. Aerosol particles, such as dust, when suspended in a gas with a temperature gradient, experience a force in the trend to the temperature gradient. Thermophoretic velocity is the velocity achieved by the particles and thermophoretic force is the force practiced by the suspended particles attributable to the temperature gradient. The quantities of thermophoretic force and thermophoretic velocity are commensurate with the temperature gradient and based on thermal conductivity of aerosol particles, thermophoretic coefficient, heat capacity of the gas and the transporter gas. Little micron sized particles are located on cold surfaces attributable to thermophoresis. In this procedure, the dissonance of particles from hot placement also takes place and a particle-free layer is noted around hot objects. This phenomenon has several sensible applications in filtration in gas cleansing, microelectronics manufacture, scattering the particulate material deposition turbine blades and particle surfaces created by condensation the vapor-gas mixtures. However, thermophoresis phenomenon was first introduced by Tyndall [20] when he noted a dust free zone in a dusty gas around a hot body. Hales *et al*. [10] have analyzed the thermophoretic deposition in geometry of engineering by studying the aerosol transport in a naturally-convected boundary layer. Garg and Jayaraj [9] have examined the thermophoretic deposition of aerosol particles due to the impingement of laminar slot jet over an inclined plate. Chiou [5] reported similarity solutions to study the effects of thermophoresis on submicron particle deposition from a forced laminar boundary layer flow onto an isothermal moving plate in a stationary incompressible fluid.Tsai and Liang [19] have obtained self-similar solutions for boundary layer flows to improve a rational correlation for estimating the influence of thermophoresis on aerosol deposition from laminar flow system. Chamkha and Pop [3] investigated the effect of thermophoresis particle deposition on heat and mass transfer by free convection from a vertical flat plate embedded in a porous medium. Walsh *et al*. [22] have analyzed the thermophoretic deposition of aerosol particles from mixed laminar tube flow with a cooled surface. Chamkha *et al*. [4] have studied the heat and mass transfer by free convection flow over a flat surface embedded in a porous medium in the presence of thermophoretic effect. EL-Hakiem *et al*. [7] have discussed the combined heat and mass transfer with the effects of thermophoresis on non-Darcy natural convection in a fluid saturated porous medium with thermal radiation effect. Muhaimin *et al*. [12] have considered the problem of two-dimensional mixed convection flow of viscous fluid with heat and mass transfer with the thermophoresis effect. Ganesan *et*

al. [8] have analyzed the influence of thermophoresis in a doubly stratified free convective flow along a vertical plate.
On the other side, investigations of radiative heat transfer play an apparent role in adjusting and dominant the heat transfer process in polymer processing industry. The quality of final product in the industry bases on the heat dominant factors. Additionally, the influences of thermal radiation on flow and heat transfer phenomena are significant in the design of several advanced energy convection systems acting at high temperature. The emission of hot walls and the operating fluid result in the form of thermal radiation. The thermal radiative effects are more beneficial when the difference between ambient temperature and the surface is bigger. The radiation effects are quite prominent in the design and producing of pertinent equipment. Recent advancements in hypersonic flights, gas cooled nuclear reactors and nuclear energy plants, gas turbines and space vehicles are several implementations of radiative heat transfer. The combined thermal radiation and mixed convection from a permeable vertical surface in a non-Darcy porous medium was examined by Murthy *et al*. [13]. Rashad [17] reported numerical solutions for the effects of thermal radiation and thermophoresis particle deposition on heat and mass transfer by steady free convection over vertical flat plate embedded in a porous medium. Duwairi and Damseh [6] have considered the thermophoresis-thermal radiation interaction on mixed-convection heat and mass transfer problem from vertical surfaces embedded in saturated porous medium. Bakier and Gorla [2] analyzed the influences of radiation and thermophoresis and in a viscous fluid over a semi-infinite vertical plate. The problem of MHD flow of viscous fluid over an inclined surface in the presence of thermophoretic and radiation effects was performed by Noor *et al*. [15]. Alam and Rahman [1] studied the effects of thermal radiation and thermophoretic particle deposition on unsteady heat and mass transfer flow pass an infinite inclined surface. Shehzad *et al*. [18] analyzed the effects of thermophoresis and thermal radiation in two dimensional mixed convection boundary layer flow of Jeffery fluid over a linearly stretching surface. Shehzad *et al*. [7] have also investigated the thermophoresis particle deposition on heat and mass transfer by mixed convection three-dimensional radiative flow of an Oldroyd-B fluid.
The aim of present investigation is to examine the effects of the thermophoresis and thermal radiation on heat and mass transfer by mixed convection over a vertical rotating cone embedded in saturated porous medium. The governing partial differential equations are transformed into a similar form and then solved numerically using the Runge-Kutta method and Newton-Raphson method. Graphical results for tangential and azimuthal skin friction coefficients, wall thermophoretic velocity, local Nusselt number and Sherwood numbers under the effect of different dimensionless groups are presented and discussed in detail.The problem is formulated in section- 2.2. Section- 2.3 contains the numerical solution. Results and discussions are presented in section- 2.4. The concluding remarks are given in section- 2.5 and the references are in section 2.6.

2. Formulation of the problem

We consider steady, laminar, two-dimensional viscous incompressible flow over a vertical rotating cone in a fluid saturated porous medium. Fig. 2.1 shows physical configuration. Here we consider curvilinear coordinate system to describe the flow configuration. The surface of the cone is maintained with the variable temperature and concentration, which are higher than ambient fluid temperature and concentration. The fluid is assumed to be gray, emitting and absorbing medium but not scattering. All the fluid and the porous medium properties are assumed to be constant except the density in buoyancy force term in the momentum equations.

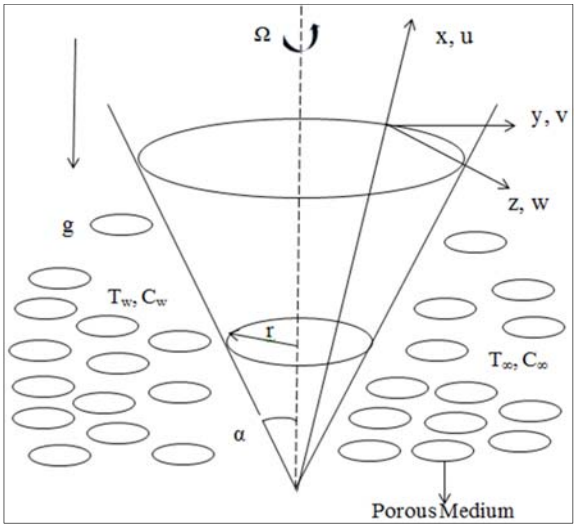

Fig. 2.1: Physical configuration and coordinate system

We assume that the fluid and the porous medium are to be locally thermodynamic equilibrium with solid matrix. Using the above assumptions and boundary layer and Boussinesq approximations the governing boundary layer equations for conservation of mass, momentum, energy and species are as follows:

$$\frac{\partial u}{\partial x}+\frac{\partial w}{\partial z}+\frac{u}{x}=0 \tag{2.1}$$

$$\rho\left(u\frac{\partial u}{\partial x}+w\frac{\partial u}{\partial z}-\frac{v^2}{x}\right)=\mu\frac{\partial^2 u}{\partial z^2}-\frac{\mu}{K}u+\rho g\beta_T\left(T-T_\infty\right)\cos(\alpha)+\rho g\beta_C\left(C-C_\infty\right)\cos(\alpha) \tag{2.2}$$

$$\rho\left(u\frac{\partial v}{\partial x}+w\frac{\partial v}{\partial z}+\frac{uv}{x}\right)=\mu\frac{\partial^2 v}{\partial z^2}-\frac{\mu}{K}v \tag{2.3}$$

$$\left(u\frac{\partial T}{\partial x}+w\frac{\partial T}{\partial z}\right)=\frac{k_e}{\rho c_p}\frac{\partial^2 T}{\partial z^2}-\frac{1}{\rho c_p}\frac{\partial q_r}{\partial z} \tag{2.4}$$

$$u\frac{\partial C}{\partial x}+w\frac{\partial C}{\partial z}+\frac{\partial}{\partial z}\left(Cv_t\right)=D\frac{\partial^2 C}{\partial z^2} \tag{2.5}$$

The corresponding boundary conditions

(i) On the surface of the cone (z = 0)

$u=0, v=r\Omega, w=0,$ (no slip at the surface)

$T=T_w(x),\ C=C_w(x)$ (Surface temperature and concentration) (2.6a)

(ii) In the free stream region $z \to \infty$

$$u = 0,\ \ v = 0,\ \ T = T_\infty,\ \ C = C_\infty \qquad (2.6b)$$

where x-axis is along a meridional section, y-axis is along a circular section and the z-axis is normal to the cone surface, u, v andware the velocity components along the tangential (x), circumferential or azimuthal (y) and normal (z) directions respectively, r is radius of the cone, Ω is the angular velocity of the rotation, ρ is the fluid density, μ is the dynamic viscosity, K is the permeability of the porous medium, c_p is the specific heat at constant pressure, g is the acceleration due to gravity, β_T and β_C are the thermal and concentration coefficients, α is the cone apex half angle, k_e is the effective thermal conductivity, q_r is the radiative heat flux and D is the molecular diffusivity.

According to Rosseland approximation the radiative heat flux q_r for an optically thick boundary layer is;

$$q_r = -\frac{4\sigma^*}{3k^*}\nabla T^4 \qquad (2.7)$$

Where k^* and σ^* are respectively the mean absorption coefficient and the Stefan-Boltzmann constant. The fluid-phase temperature differences within the flow are assumed to be sufficiently small such that T^4 may be expressed as a linear function of the temperature. This is accomplished by expanding in a Taylor series about T_∞ and neglecting higher order terms to yield

$$T^4 \cong 4T_\infty^3 T - 3T_\infty^4 \qquad (2.8)$$

Using eqns. (2.7) and (2.8), eqn. (2.44) reduces to

$$\left(u\frac{\partial T}{\partial x} + w\frac{\partial T}{\partial z}\right) = \frac{k_e}{\rho c_p}\frac{\partial^2 T}{\partial z^2} + \frac{1}{\rho c_p}\frac{16\sigma^* T_\infty^3}{3k^*}\frac{\partial^2 T}{\partial z^2} \qquad (2.9)$$

And the thermophoretic velocity v_t which appear in eqn. (2.5) recommended by Talbot *et al*. [69] is defined as

$$v_t = -k\nu\frac{\partial T}{\partial z} \qquad (2.10)$$

Where k is the thermophoretic coefficient whose values range from 0.2 and 1.2 and $k\nu$ is the thermophoretic diffusivity.

2.1. Non-dimensionalisation

To obtain the non-dimensional governing boundary layer equations we introduce the following non-dimensional transformations:

$$\eta = \left(\frac{\Omega\sin(\alpha)}{\nu}\right)^{1/2} z,\ u = x\Omega\sin(\alpha)F(\eta),$$
$$v = x\Omega\sin(\alpha)G(\eta),\ \ r = x\sin(\alpha)$$
$$w = \left(\nu\Omega\sin(\alpha)\right)^{1/2} H(\eta),\ \theta(\eta) = \frac{T - T_\infty}{T_w - T_\infty},\ \phi(\eta) = \frac{C - C_\infty}{C_w - C_\infty}$$
$$T_w(x) - T_\infty = \frac{(T_L - T_\infty)x}{L},\ C_w(x) - C_\infty = \frac{(C_L - C_\infty)x}{L} \qquad (2.11)$$

where (L) is the cone slant height, T_L is the cone surface temperature and C_L is the concentration at the cone base (x = L).Substituting Eqns. (2.10) and (2.11) in Eqs. (2.1) – (2.3), (2.5) and (2.9), the following non-dimensional equations are obtained:-

$$F = -\frac{1}{2}H' \qquad (2.12)$$

$$H''' - HH'' + \frac{H'^2}{2} - Da^{-1}H' - 2G^2 - 2g_s(\theta + N\phi) = 0 \qquad (2.13)$$

$$G'' - HG' + H'G - Da^{-1}G = 0 \qquad (2.14)$$

$$\frac{1}{\Pr}\theta''\left(1 + \frac{4}{3}R\right) + \left(\frac{1}{2}H'\theta - H\theta'\right) = 0 \qquad (2.15)$$

$$\phi'' + Sc\left(\frac{1}{2}H'\phi - H\phi'\right) + \frac{Sc\,k\,Nt}{Nt\,\theta + 1}\left(\phi'\theta' + \phi\theta'' - \frac{Nt\,\phi\theta'^2}{Nt\theta + 1}\right) = 0 \qquad (2.16)$$

Where

$Da^{-1} = \dfrac{\nu}{K\Omega\sin\alpha}$ is the inverse of Darcy number,

$Gr = \dfrac{g\beta_T(T_w - T_\infty)L^3\cos\alpha}{\nu^2}$ is the Grashof number,

$N = \dfrac{\beta_C(C_w - C_\infty)}{\beta_T(T_w - T_\infty)}$ is the buoyancy ratio,

$\mathrm{Re} = \dfrac{\Omega L^2\sin\alpha}{\nu}$ is the local Reynolds number,

$g_s = \dfrac{Gr}{\mathrm{Re}^2}$ is the mixed convection parameter,

$\Pr = \dfrac{\mu C_p}{k_e}$ is the Prandtl number,

$Sc = \dfrac{\nu}{D}$ is the Schmidt number,

$R = \dfrac{4\sigma^* T_\infty^3}{k^* k_e}$ radiation parameter,

$Nt = \dfrac{T_w - T_\infty}{T_\infty}$, is the relative temperature difference parameter.

The transformed boundary conditions are

$$\begin{aligned} &H = 0,\ H' = 0,\ G = 1,\quad \theta = 1,\quad \phi = 1 \quad \text{at } \eta = 0 \\ &H' = 0,\ G = 0,\quad \theta = 0,\quad \phi = 0 \qquad\quad \text{as } \eta \to \infty \end{aligned} \qquad (2.17)$$

The main objective of the present study is to find the parameters of physical interest in fluid flow, heat and mass transport problems which are the local surface skin friction coefficients in x (tangential) and y (azimuthal) directions, local Nusselt number and local Sherwood number.

$$C_{fx} = \frac{2\mu\left(\frac{\partial u}{\partial z}\right)_{z=0}}{\rho\left(\Omega_0 x\sin\alpha\right)^2},\ C_{fy} = \frac{-2\mu\left(\frac{\partial v}{\partial z}\right)_{z=0}}{\rho\left(\Omega_0 x\sin\alpha\right)^2},$$
$$Nu_x = \frac{-x\left(\frac{\partial T}{\partial z}\right)_{z=0}}{(T_w - T_\infty)},\ Sh_x = \frac{-x\left(\frac{\partial C}{\partial z}\right)_{z=0}}{(C_w - C_\infty)} \qquad (2.18)$$

These parameters are given by these parameters can be written in non-dimensional form as follows:-

Skin friction coefficient in x-direction

$$\mathrm{Re}^{1/2}C_{fx} = -H''(0) \qquad (2.19)$$

Skin friction coefficient in y-direction

$$2^{-1}\mathrm{Re}^{1/2}C_{fy} = -G'(0) \qquad (2.20)$$

Local Nusselt number

$$\mathrm{Re}^{-1/2}Nu_x = -\theta'(0) \qquad (2.21)$$

Local Sherwood number

$$\mathrm{Re}^{-1/2}Sh_x = -\phi'(0) \qquad (2.22)$$

3. Method of solution

The set of equations (2.12)-(2.16) concerning boundary value problems pertinent to vertical rotating cone are coupled, nonlinear ordinary differential equations, which are difficult to solve analytically, therefore we approach suitable numerical method, namely shooting technique. Hence, in order to solve (2.12) – (2.16) with the boundary conditions (2.17) we used shooting technique (see Murthy et.al [40], Srinivasacharya et.al [65, 66] and Mallikarjuna et.al [37]) that use Runge-Kutta method and Newton-Raphson method. The main steps involved in this method are as follows:

Step-1: Transforming Higher order equations into first order equations

In this, first eqns. (2.12) - (2.16) are converted into a system of differential equations of first order, by assuming $H = X_1,\ G = X_4,\ \theta = X_6,\ \phi = X_8,$ we get

$$H' = \frac{dX_1}{d\eta} = X_2, \tag{2.23}$$

$$H'' = \frac{dX_2}{d\eta} = X_3, \tag{2.24}$$

$$H''' = \frac{dX_3}{d\eta} = X_1X_3 - \frac{1}{2}X_2^2 + Da^{-1}X_2 + 2X_4^2 + 2g_s\left(X_6 + NX_8\right) \tag{2.25}$$

$$G' = \frac{dX_4}{d\eta} = X_5, \tag{2.26}$$

$$G'' = \frac{dX_5}{d\eta} = X_1X_5 - X_2X_4 + Da^{-1}X_4 \tag{2.27}$$

$$\theta' = \frac{dX_6}{d\eta} = X_7, \tag{2.28}$$

$$\theta'' = \frac{dX_7}{d\eta} = \frac{\Pr}{\left(1+4R/3\right)}\left(X_1X_7 - \frac{1}{2}X_2X_6\right) \tag{2.29}$$

$$\phi' = \frac{dX_8}{d\eta} = X_9 \tag{2.30}$$

$$\phi'' = \frac{dX_9}{d\eta} = Sc\left(X_1X_9 - \frac{1}{2}X_2X_8\right) - \frac{ScNt}{1+X_6Nt}\left(X_7X_9 + \frac{X_8\Pr}{\left(1+4R/3\right)}\left(X_1X_7 - \frac{1}{2}X_2X_6\right) - \frac{X_8X_7^2Nt}{1+NtX_6}\right) \tag{2.31}$$

With boundary conditions

$$X_1(0) = 0, X_2(0) = 0, X_4(0) = 1, X_6(0) = 1, X_8(0) = 1,$$
$$X_2(\infty) = 0, X_4(\infty) = 0, X_6(\infty) = 0, X_8(\infty) = 0 \tag{2.32}$$

Step-2: Decision on ∞

The infinite value $\eta = \infty$ can be chosen large enough, so that a suitable change in the solution is observed for η larger than $\eta = \infty$.

Step-3: Converting boundary value problem (BVP) into initial value problem (IVP)

We convert BVP (2.23)-(2.31) into initial value problem by choosing suitable initial conditions for $X_3(0),\ X_5(0),\ X_7(0),\ X_9(0)$, which are not specified at $\eta = 0$ .That is $X_3(0) = 0.5,\ X_5(0) = 0.5,\ X_7(0) = -0.5,\ X_9(0) = -0.5$.

Step-4: Integrate the IVP

The eqns. (2.23)-(2.31) are integrated using fourth order Runge-Kutta method from $\eta = 0$ to $\eta_{\max}$ over successive step lengths $\Delta\eta$, where $\eta_{\max}$ is η at ∞ and chosen large enough so that a suitable change in the solution is observedfor η larger than $\eta_{\max}$. We employed ODE45 solver in MATLAB to solve these nine first ordered coupled nonlinear ordinary differential equations. The accuracy of the assumed values for $X_3(0),\ X_5(0),\ X_7(0),\ X_9(0)$ is then checked by comparing the calculated values of X_2, X_4, X_6, X_8 at $\eta = 0$ with their given value at $\eta = \infty$. If a difference exists, another set of initial values for $X_3(0),\ X_5(0),\ X_7(0),\ X_9(0)$ is assumed and the process is repeated.

Step-5: Employing Newton-Raphson method to accurately predict initial conditions

Newton-Raphson method for solving nonlinear equations involves an iterative process of iteratively refining x, by a correction, h

$$X_{i+1} = X_i + h \tag{2.33}$$

where h is calculated by linear extrapolation of the function, f(x) to zero.

$$0 = f\left(X_i\right) + \left(\frac{df}{dx}\right)_{X_i} h \tag{2.34}$$

This approach can be scaled up readily to solve the roots of coupled equations. For the present problem the equations in matrix form are

$$\begin{pmatrix} X_3(\eta=0)_{i+1} \\ X_5(\eta=0)_{i+1} \\ X_7(\eta=0)_{i+1} \\ X_9(\eta=0)_{i+1} \end{pmatrix} = \begin{pmatrix} X_3(\eta=0)_i \\ X_5(\eta=0)_i \\ X_7(\eta=0)_i \\ X_9(\eta=0)_i \end{pmatrix} + \begin{pmatrix} h_1 \\ h_2 \\ h_3 \\ h_4 \end{pmatrix} \tag{2.35}$$

where $\left(h_1\ h_2\ h_3\ h_4\right)^T$ is the solution of the problem.

$$\begin{pmatrix} 0 \\ 0 \\ 0 \\ 0 \end{pmatrix} = \begin{pmatrix} X_3(\eta=10)_i \\ X_5(\eta=10)_i \\ X_7(\eta=10)_i \\ X_9(\eta=10)_i \end{pmatrix} + \begin{pmatrix} \left(\frac{dH(\eta=10)}{dX_3(\eta=0)}\right)_{X_9} & \left(\frac{dH(\eta=10)}{dX_5(\eta=0)}\right)_{X_7} & \left(\frac{dH(\eta=10)}{dX_7(\eta=0)}\right)_{X_5} & \left(\frac{dH(\eta=10)}{dX_9(\eta=0)}\right)_{X_3} \\ \left(\frac{dG(\eta=10)}{dX_3(\eta=0)}\right)_{X_9} & \left(\frac{dG(\eta=10)}{dX_5(\eta=0)}\right)_{X_7} & \left(\frac{dG(\eta=10)}{dX_7(\eta=0)}\right)_{X_5} & \left(\frac{dG(\eta=10)}{dX_9(\eta=0)}\right)_{X_3} \\ \left(\frac{d\theta(\eta=10)}{dX_3(\eta=0)}\right)_{X_9} & \left(\frac{d\theta(\eta=10)}{dX_5(\eta=0)}\right)_{X_7} & \left(\frac{d\theta(\eta=10)}{dX_7(\eta=0)}\right)_{X_5} & \left(\frac{d\theta(\eta=10)}{dX_9(\eta=0)}\right)_{X_3} \\ \left(\frac{d\phi(\eta=10)}{dX_3(\eta=0)}\right)_{X_9} & \left(\frac{d\phi(\eta=10)}{dX_5(\eta=0)}\right)_{X_7} & \left(\frac{d\phi(\eta=10)}{dX_7(\eta=0)}\right)_{X_5} & \left(\frac{d\phi(\eta=10)}{dX_9(\eta=0)}\right)_{X_3} \end{pmatrix} \begin{pmatrix} h_1 \\ h_2 \\ h_3 \\ h_4 \end{pmatrix} \tag{2.36}$$

These equations are designed to find initial values of X_3, X_5, X_7, X_9 that satisfy final values of H, G, θ, ϕ at $\eta = \infty$. Equations (2.35) and (2.36) can be expressed using the matrix and vector variable as

$$W_{i+1} = W_i + h \tag{2.37}$$

And

$$0 = F + Kh \tag{2.38}$$

Respectively, and combined to reach an iterative process

$$W_{i+1} = W_i - K^{-1}F \tag{2.39}$$

Where K is the Jacobian matrix. Although the sixteen derivatives that comprise in K cannot be expressed analytically, they can be approximated by two-term finite

divided differences. The first of the sixteen is estimated by the equation

$$\left(\frac{dH(\eta=10)}{dX_3(\eta=0)}\right)_{(X_5,X_7,X_9)} = \frac{H(\eta=10)_{(X_3+dX_3,X_5,X_7,X_9)} - H(\eta=10)_{(X_3,X_5,X_7,X_9)}}{dX_3} \tag{2.40}$$

To find the approximation values for sixteen derivatives, the ODEs in (2.23) – (2.31) are to be solved for four 4-tuple of initial values (X_3, X_5, X_7, X_9), $(X_3 + dX_3, X_5, X_7, X_9)$, $(X_3, X_5 + dX_5, X_7, X_9)$, $(X_3, X_5, X_7 + dX_7, X_9)$ and $(X_3, X_5, X_7, X_9 + dX_9)$, where dX_3, dX_5, dX_7 and dX_9 are small numbers.

At first, the ordinary differential equations (2.23)-(2.31) are solved in the interval $0 \le \eta \le \eta_{\max}$ for four 4-tuples of initial values, where $dX_3 = 0.01, dX_5 = 0.01, dX_7 = 0.01,$ and $dX_9 = 0.01$. The calculated values of X_3, X_5, X_7, X_9 for each 4-tuple of initial conditions are placed into an array (W_1, W_2, W_3, W_4).

Second, the sixteen derivatives involved in K are evaluated. Third, new approximations of initial values are evaluated from (2.39). This process is continuous until the magnitude of the both corrections within 10^{-6}. The accuracy of the solution is enhanced by taking dX_3, dX_5, dX_7 and dX_9 to reduce as the solution converge.

4. Results and discussions

In order to get a clear insight of the physical problem, numerical results for the local skin friction coefficients in the tangential and azimuthal directions, local Nusselt number, local Sherwood number, and wall thermophoretic velocity are presented with the help of graphical illustrations. The results are given through a parametric study showing the effects different dimensionless parameters, namely, of Darcy number and thermal radiation parameter R, and thermophoretic coefficient k. These conditions are intended for the value of Prandtl number (*Pr*) is taken to be 0.71 which corresponds to air and the value of Schmidt number (*Sc*) is chosen to represent hydrogen at 25^0C and 1 atm. The dimensionless buoyancy parameter g_s take the value 30, which corresponds to the problem entire mixed convection regime, and the corresponding parameter *N* takes the value both aiding and opposing flows. The results of this parametric study are shown in figures.

Figs. 2.2- 2.4 illustrate the variation of tangential, circumferential and normal velocity profiles for different values of inverse Darcy parameter (Da^{-1}) respectively. Increase in inverse Darcy parameter causes an enhancement in viscosity effect in boundary layer regime. This leads to reduce the fluid flow rate over the boundary layer. Hence tangential velocity profile retards considerably, decrease velocity boundary layer thickness for larger values of inverse Darcy parameter as shown in fig.2.2. We notice depreciation in circumferential velocity profile with rise in inverse Darcy number as given in fig. 2.3. Conversely, normal velocity profiles reported opposite results as increase in inverse Darcy number (fig. 2.4).

Figs. 2.5 and 2.6 show the variation of temperature and concentration distributions for different values of inverse Darcy number (Da^{-1}). As observed in fig. 2.2, volume flow rate of the fluid is increased in boundary layer regime, transfer of heat is increased. Temperature distribution therefore boosted, i.e. increasing thermal boundary thickness for larger values of inverse Darcy number. Concentration distribution reported similar results, i.e. increase in solutal boundary layer thickness.

Figs. 2.7 – 2.11 depict the variation of tangential, circumferential and normal velocity profiles for different values of inverse Darcy number (Da^{-1}). Increasing radiation parameter R accelerates strongly, i.e., increases the fluid tangential velocity while circumferential and normal velocity profiles reduce. Increasing thermal radiation contribution with an increase in R values strengthens the thermal diffusivity of the fluid regime and enhances the thermal energy in the thermal boundary layer. Temperature profiles are therefore increased for larger values of R, as shown in fig. 2.10. Both velocity and thermal boundary layer thicknesses are increased with increasing contribution from thermal radiation (with decreasing contribution from thermal conduction). Conversely, there is considerable decrement in concentration distribution for larger values of R, as observed in fig. 2.11.

Figs. 2.12 – 2.16 depict the variations of tangential skin-friction coefficient (or $-H''(0)$) and azimuthal skin-friction coefficient (or $-G'(0)$), local Nusselt number (or $-\theta'(0)$), local Sherwood number(or $-\phi'(0)$), anddimensionless wall thermophoretic velocity (or V_{tw}) with different values of Darcy number *Da* for both aiding and opposing flows $(N > 0 \text{ and } N < 0)$, respectively. It is known that the presence of a porous medium in the flow presents a reluctance to flow. Thus, this reluctant force tends to decelerate the motion of the fluid along the cone surface. As the result of a causing a deceleration in the flow with an increase in the inverse Darcy number *Da* induces a significant reduction in both the tangential skin-friction coefficient $-H''(0)$ and wall thermophoretic velocity V_{tw} and a pronounced enhancement in the azimuthal skin-friction coefficient $-G'(0)$, local Nusselt number $-\theta'(0)$, and Sherwood number, $-\phi'(0)$ for both aiding and opposing flows.This means that the presence of porous medium causes higher restriction to the fluid, which diminishes the primary fluid flow and boosts the secondary of the fluid flow.

The effect of the thermal radiation R on the tangential skin-friction coefficient $-H''(0)$, azimuthal skin-friction coefficient $-G'(0)$, local Nusselt number -θ'(0), local Sherwood number $-\phi'(0)$, andwall thermophoretic velocity V_{tw} are respectively shown in Figs. 2.17 – 2.21. From these figures, it can be seen that the increasing in thermal radiation Rleads to a significant reduction in the local Nusselt number $-\theta'(0)$. This behavior produces a more pronounced enchantment in the local skin-friction coefficients, local Sherwood number or thewall thermophoretic velocity. The reason for this trend can be explained as follows, the specific effect of the radiation parameter *R*is to enhance the temperature gradient at the cone surface and thereby contribute to decrease the heat transfer rate. However, larger values of R imply smaller values of local Nusselt number. This may be related to the fact that the raise of the values of *R* implies more interaction of radiation with the thermal boundary layers and consequently the heat absorption intensity of the fluid boosts.

On the other hand, it can be seen from Figs. 2.12- 2.21 that positive values of the buoyancy ratio *N* correspond to aiding

flow while negative values of *N* correspond to opposing flow. In addition, an increment in the values of *N* has a tendency to promote the buoyancy effects due to concentration difference. This produces more flow along the cone surface causing the local skin-friction coefficients, Nusselt and Sherwood numbers to enhance as shown in figures 2.12 – 2.15 and 2.17 – 2.20. This increase in the skin-friction coefficients occurs at the expense of thewall thermophoretic velocity, which decrease strongly as *N* increases as evident from figures 2.16and2.21. Furthermore, it is noted that a rise in the thermophoretic coefficient k clearly induces a marked drop in both the thewall thermophoretic velocity and local Sherwood number, while an insignificant behavior occurs in both the local skin-friction coefficients, Nusselt number. In the absence of mass transfer with thermophoresis, thermal radiation and inverse Darcy parameter the nonlinear ordinary differential equations (2.23)-(2.31) with corresponding boundary conditions (2.32) exactly coincides with those of Hering and Grosh [32] and Himasekhar et.al [33]. The comparison results found very good agreement with earlier existing results as shown in Tables 2.1 and 2.2, respectively.

Table 2.1. The values of $-H''(0), -G'(0)$ and $-\theta'(0)$ for different values of $g_s = \frac{Gr}{\mathrm{Re}^2}$ for $\mathrm{Pr} = 0.7$, $Da^{-1} = 0$, $R = 0$ and $N = 0$ (in the absence of concentration equation).

g_s	Results of Hering and Grosh [32]			The results of present study		
	-H″(0)	-G′(0)	-θ′ (0)	-H″ (0)	-G′(0)	-θ′ (0)
0	1.0205	0.61592	0.42852	1.0203	0.61583	0.42842
1.0	2.2078	0.85076	0.61202	2.2075	0.85080	0.61213
100	46.052	2.4738	1.7946	46.0523	2.47382	1.79459

Table 2.2.: The values of $-H''(0), -G'(0)$ and $-\theta'(0)$ for different values of Pr for $g_s = 0.1$, $Da^{-1} = 0$ and $N = 0$ (in the absence of concentration equation).

Pr	Results of Himasekhar *et al.* [33]			Results of present study		
	-H″(0)	-G′(0)	-θ′ (0)	-H″ (0)	-G′(0)	-θ′ (0)
1.0	1.1282	0.6437	0.5457	1.12824	0.64374	0.54573
2.0	1.1120	0.6335	0.7450	1.11203	0.63347	0.74502
10	1.0702	0.6202	1.4106	1.07018	0.62021	1.41066

5. Conclusions

The effects of the various relevant parameters namely the Darcy number, thermal radiation parameter and thermophoretic coefficient on the local skin friction coefficients in the tangential and azimuthal directions, wall thermophoretic velocity, local Nusselt Sherwood numbers are shown graphically and discussed.

- From the obtained results of the problem, it was found that an increasing in the values of Darcy number resulted in a pronounced increase in the azimuthal skin-friction coefficient, local Nusselt and Sherwood numbers, for both aiding and opposing flows whereas the effects reverse significantly with both the tangential skin-friction coefficient and wall thermophoretic velocity.
- Increase in the thermal radiation parameter causes an enhancement in local skin-friction coefficients, local Sherwood number or thewall thermophoretic velocity, whereas the opposite trend happened with the local Nusselt number.

Finally, both the wall thermophoretic velocity and local Sherwood number are reduced as the thermophoretic coefficient increased, while unaffected behavior is noted for the local skin-friction coefficients and Nusselt number.

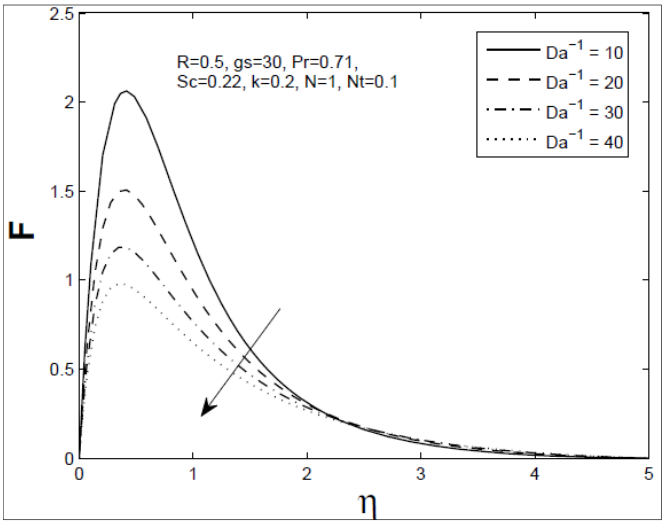

Fig 2.2. Tangential velocity profile (F) for different values of inverse Darcy number (Da^{-1})

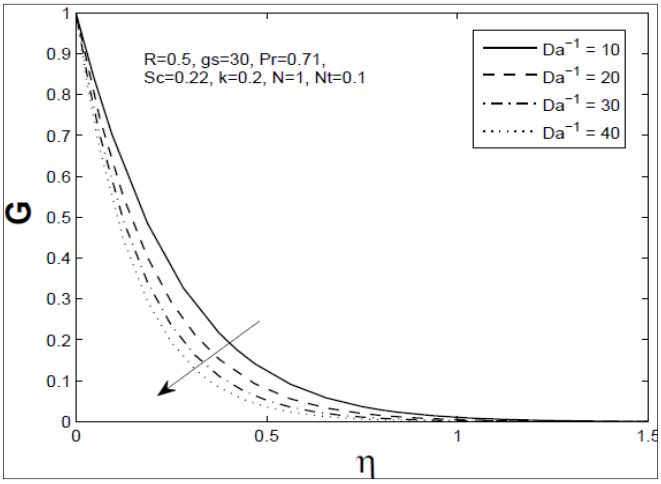

Fig 2.3. Circumferential velocity profile (G) for different values of inverse Darcy number (Da^{-1})

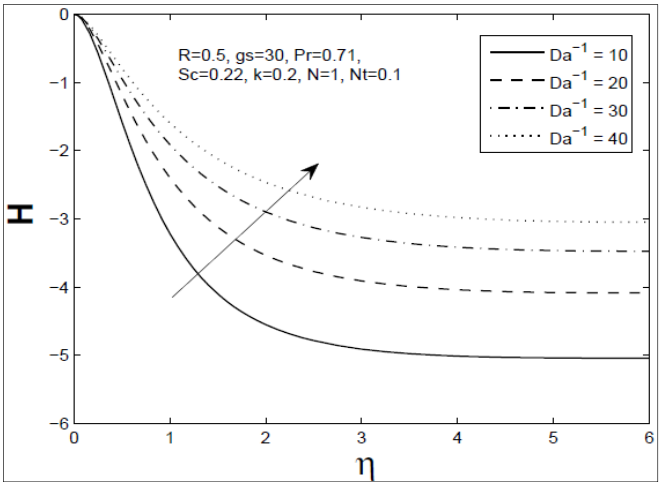

Fig 2.4. Normal velocity profile (H) for different values of inverse Darcy number (Da^{-1})

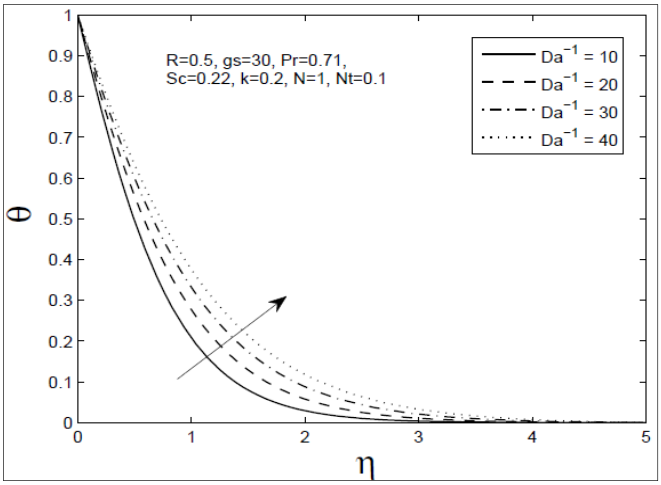

Fig 2.5. Temperature profile (θ) for different values of inverse Darcy number (Da^{-1})

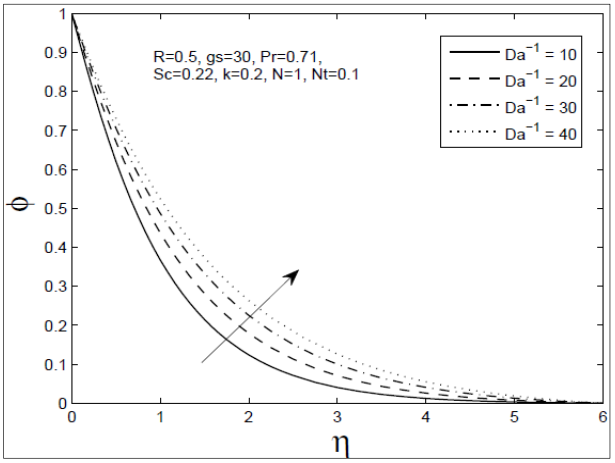

Fig 2.6. Concentration profile (ϕ) for different values of inverse Darcy number (Da^{-1})

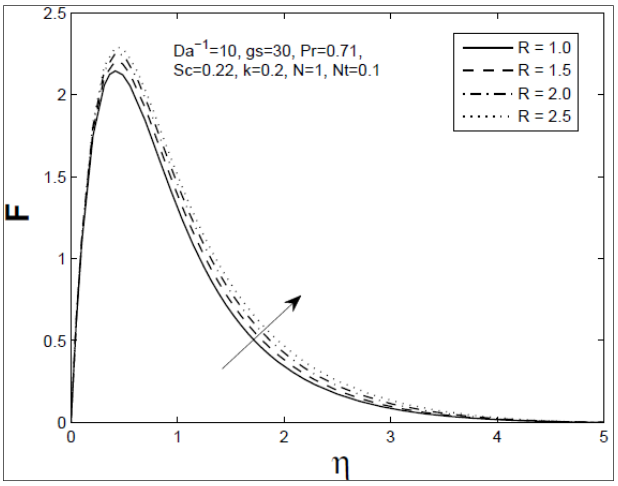

Fig 2.7. Tangential velocity profile (F) for different values of radiation parameter (R)

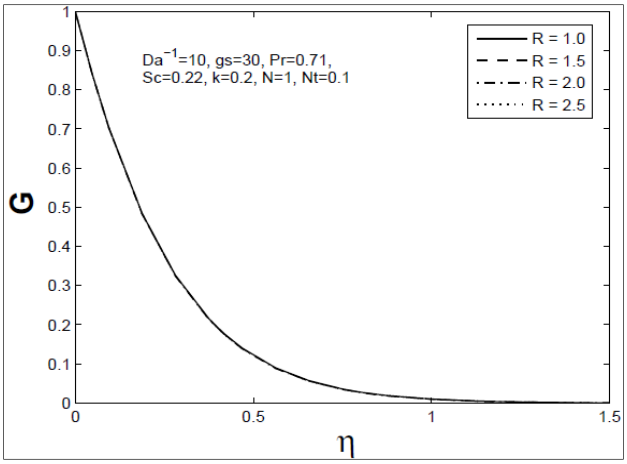

Fig 2.8. Circumferential velocity profile (G) for different values of radiation parameter (R)

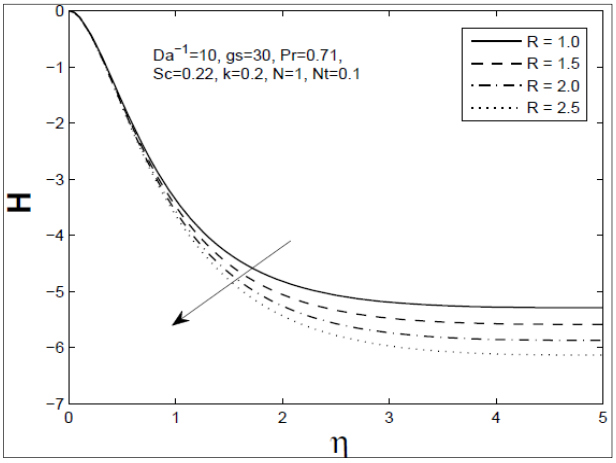

Fig 2.9. Normal velocity profile (H) for different values of radiation parameter (R)

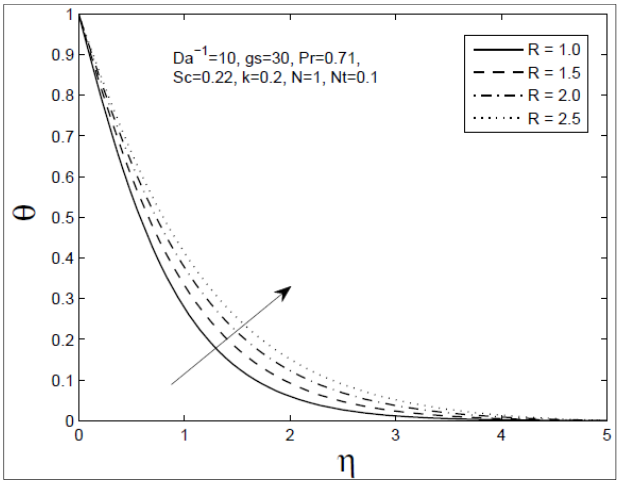

Fig 2.10. Temperature profile (θ) for different values of radiation parameter (R)

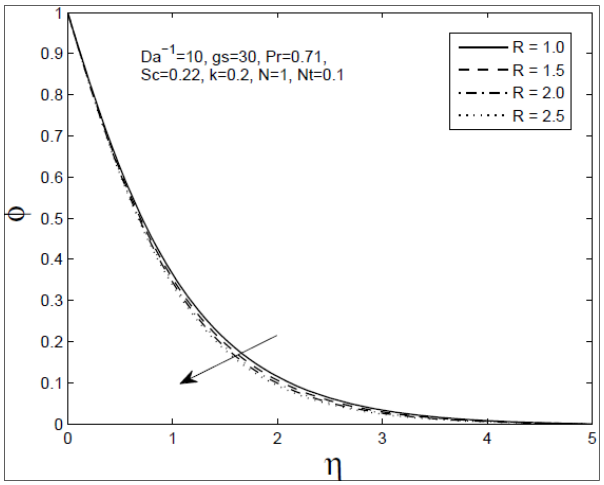

Fig 2.11. Concentration profile (ϕ) for different values of radiation parameter (R)

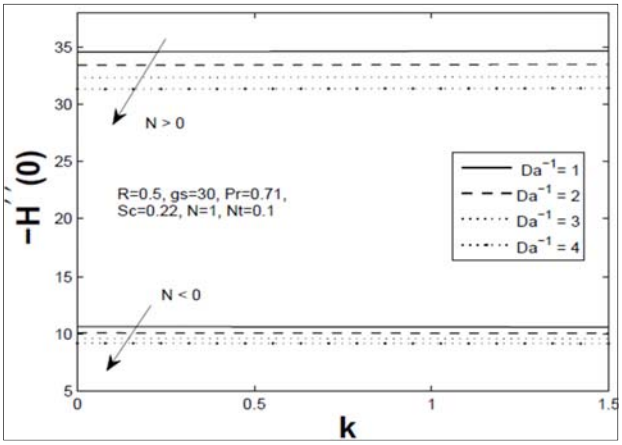

Fig 2.12. Tangential skin-friction (C_{fx}) for different values inverse Darcy number (Da^{-1})

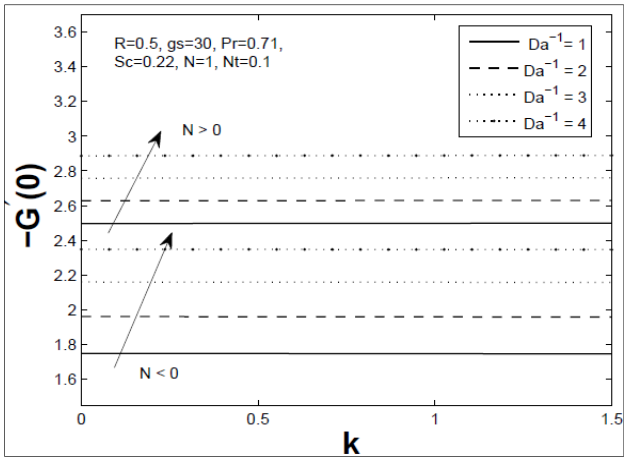

Fig 2.13. Azimuthal skin-friction (C_{fy}) for different values of inverse Darcy number (Da^{-1})

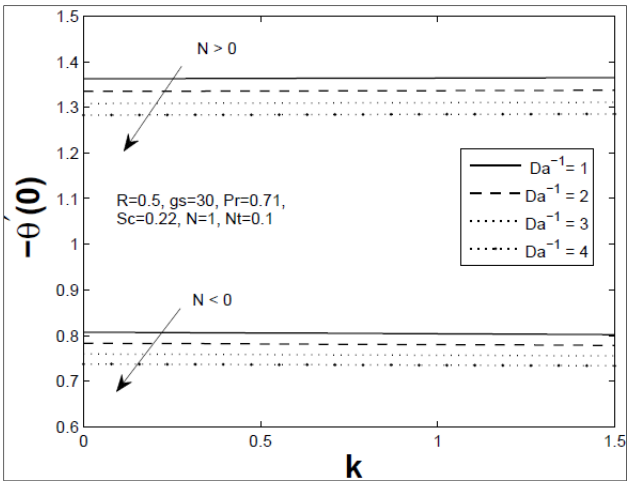

Fig 2.14. Local Nusselt number (Nu) for different values of inverse Darcy number (Da^{-1})

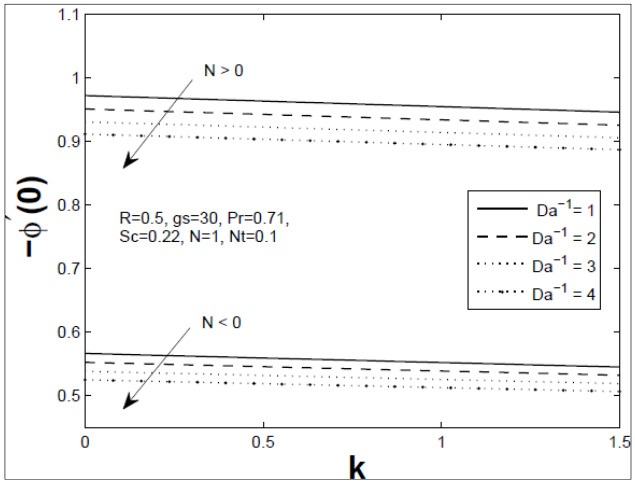

Fig 2.15. Local Sherwood number (Sh) for different values of inverse Darcy number (Da^{-1})

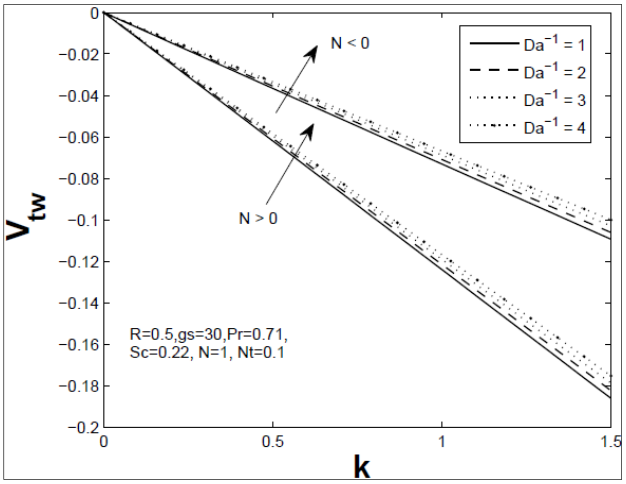

Fig 2.16. Wall thermophoretic velocity (V_{tw}) for different values of inverse Darcy number (Da^{-1})

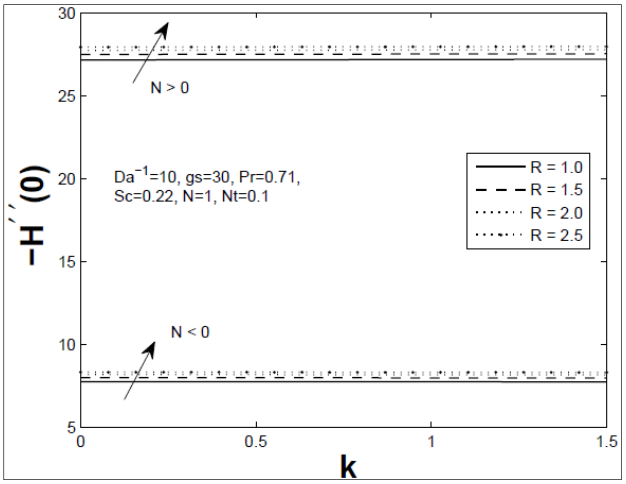

Fig 2.17. Tangential skin-friction (C_{fx}) for different values of radiation parameter (R)

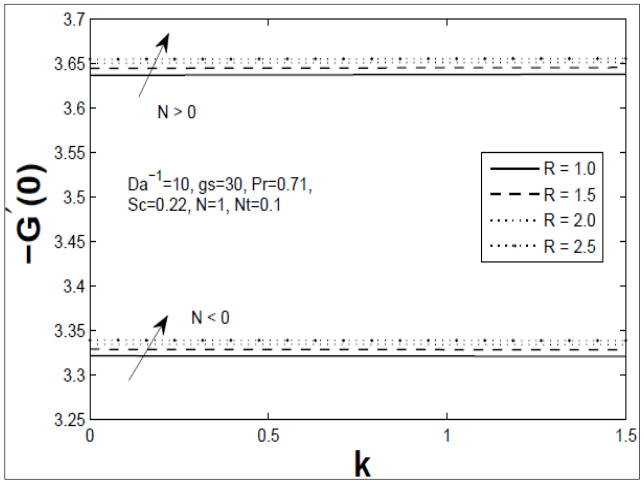

Fig 2.18. Azimuthal skin-friction (C_{fy}) for different values of radiation parameter (R)

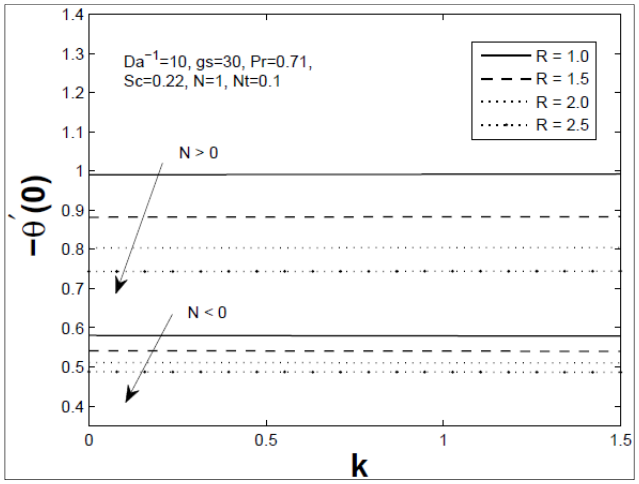

Fig 2.19. Local Nusselt number (Nu) for different values of radiation parameter (R)

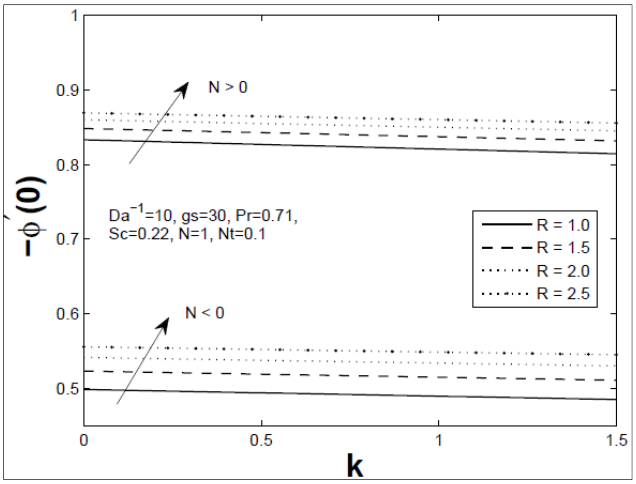

Fig 2.20. Local Sherwood number (Sh) for different values of radiation parameter (R)

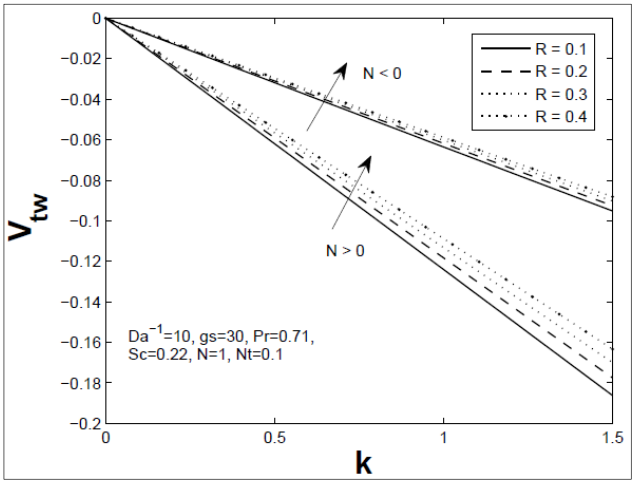

Fig 2.21. Wall thermophoretic velocity (V_{tw}) for different values of radiation parameter (R)

References

1. Alam MS, Rahman MM. Thermophoretic particle deposition on unsteady hydromagnetic radiative heat and mass transfer flow along an infinite inclined permeable surface with viscous dissipation and Joule heating. Engineering e-Transactions, 2012; 7(2):116-126.
2. Bakier AY, Gorla RSR. Effects of thermophoresis and radiation on laminar flow along a semi-infinite vertical plate. Heat Mass Transfer, 2011; 47(4):419-425.
3. Chamkha AJ, Pop I. Effect of thermophoresis particle deposition in free convection boundary layer from a vertical flat plate embedded in a porous medium, Int. Comm. Heat Mass Transfer, 2004; 31(3):421- 430.
4. Chamkha AJ, Al-Mudhaf AF, Pop I. Effect of heat generation or absorption on thermophoretic free convection boundary layer from a vertical flat plate embedded in a porous medium, International Communication in Heat and Mass Transfer, 2006; 33(9):1096-1102.
5. Chiou MC. Effects of thermophoresis on submicron particle deposition from a forced laminar boundary layer flow onto an isothermal moving plate, ActaMechanica, 1998; 129:219-229.
6. Duwairi HM, Damseh RA. Thermophoresis particle deposition-thermal radiation interaction on mixed convection from vertical surfaces embedded in porous medium, Can. J. Phys. 2009; 87:161-167.
7. EL-Hakiem MA, El-Kabeir SMM, Rashad AM. Combined heat and mass transfer on non-Darcy natural convection in a fluid saturated porous medium with thermophoresis, Int. J. Applied Mech. Eng. 2007; 12(1):9-18.
8. Ganesan P, Suganthi RK, Loganathan P. Thermophoresis particle deposition effects in a free convective doubly stratified medium over a vertical plate, Meccanica, 2014; 49(3):659-672.
9. Garg VK, Jayaraj S. Thermophoresis of aerosol particles in laminar flow over inclined plates, Int. J. Heat Mass Transfer. 1988; 31:875-890.
10. Hales JM, Schwendiman LC, Horst TW. Aerosol transport in a naturally-convected boundary layer, Int. J. Heat Mass Transfer. 1972; 15(10):1837-1849.
11. Ingham DB, Pop I. Transport phenomenon in porous media, Elsevier, Oxford, 2005, Vol. III.
12. Murthy PVSN, Mukherjee S, Srinivascharya D, Krishna PVSSSR. Combined radiation and mixed convection from a vertical wall with suction/injection in a non-Darcy porous medium, Acta Mechanica, 2004; 168:145-156.
13. Nield AD, Bejan A. Convection in porous media, 3rd ed. Springer, New York, 2006.
14. Noor NFM, Abbasbandy S, Hashim I. Heat and mass transfer of thermophoretic MHD flow over an inclined radiate isothermal permeable surface in the presence of heat source/sink, Int. J. Heat Mass Transfer. 2012; 55:2122-2128.
15. Pop I, Ingham DB. Convective Heat Transfer: mathematical and computational modelling of viscous fluids and porous media, Pergamon, Oxford, 2001.
16. Rashad AM. Influence of radiation on MHD free convection from a vertical flat plate embedded in porous media with thermophoretic deposition of particles, Commun. Nonlinear Sci. Numer. Simulat., 2008; 13(10):2213-2222.
17. Shehzad SA, Alsaedi A, Hayat T. Influence of thermophoresis and Joule heating on the radiative flow of Jeffery fluid with mixed convection, Brazilian Journal of Chemical Engineering. 2013; 30(4):897-908.
18. Tsai R, Liang LJ. Correlation for thermophoretic deposition of aerosol particles onto cold plates, J. Aerosol Sci. 2001; 32:473-487.
19. Shehzad SA, Alsaedi A, Hayat T. Influence of thermophoresis and Joule heating on the radiative flow of Jeffery fluid with mixed convection, Brazilian Journal of Chemical Engineering. 2013; 30(4):897-908.
20. Tyndall J. On dust and disease. Proc. R. Inst., 1871, 611-662.
21. Vafai K. Handbook of Porous Media, 2nd ed. Taylor & Francis, New York, 2005.
22. Walsh JK, Weimer AW, Hrenya CM. An experimental study of thermophoretic deposition of aerosol particles in laminar tube flow with mixed convection, Aerosol Sci. and Tech., 2006; 40:178-188.